ADVANCED MATERIALS
www.advmat.de

3D Printing of Living Responsive Materials and Devices

*Xinyue Liu, Hyunwoo Yuk, Shaoting Lin, German Alberto Parada, Tzu-Chieh Tang, Eléonore Tham, Cesar de la Fuente-Nunez, Timothy K. Lu, and Xuanhe Zhao**

3D printing has been intensively explored to fabricate customized structures of responsive materials including hydrogels, liquid-crystal elastomers, shape-memory polymers, and aqueous droplets. Herein, a new method and material system capable of 3D-printing hydrogel inks with programed bacterial cells as responsive components into large-scale (3 cm), high-resolution (30 μm) living materials, where the cells can communicate and process signals in a programmable manner, are reported. The design of 3D-printed living materials is guided by quantitative models that account for the responses of programed cells in printed microstructures of hydrogels. Novel living devices are further demonstrated, enabled by 3D printing of programed cells, including logic gates, spatiotemporally responsive patterning, and wearable devices.

3D printing is an emerging technology to fabricate customized structures of responsive materials that have found applications in areas as diverse as drug delivery,[1] tissue engineering,[2,3] soft actuators,[4,5] and adaptive buildings.[6] Existing stimuli-responsive materials for 3D printing include hydrogels,[4] liquid-crystal elastomers,[7] shape-memory polymers,[8] and aqueous droplets.[5] In nature, highly organized, 3D, multicellular living systems (e.g., microbial biofilms, gut microbiota, and tumor tissues) can perform complex cellular functions over time, such as cell cooperation, competition, proliferation, and apoptosis, in response to numerous spatiotemporally varying signals.[9–13] Recent developments in synthetic biology have further enabled programing of living cells to accurately respond to various stimuli such as heat, light, and chemicals.[9] 3D-printed architectures of programed cells will not only mimic highly organized, time-evolving biological constructs, but also provide new functions as living responsive materials and devices.[3,5] However, the potential benefits of harnessing programed cells as active components in 3D printing have not been well explored due to challenges of integrating programed cells into macroscopic structures with high precision while maintaining their viability and responsiveness.

Here, we report a new method and material system capable of printing programed bacterial cells into large-scale (3 cm) high-resolution (30 μm) living networks that accurately respond to signaling chemicals in a programmable manner. The design of 3D printed structures is guided by quantitative models that account for the responses of programed cells in printed microstructures. We further demonstrate novel living devices enabled by 3D printing of programed cells, including logic gates, spatiotemporally responsive patterning, and wearable devices.

The design principle for 3D printing of living materials and devices is illustrated in **Figure 1**a. On one hand, living cells as responsive components can be genetically engineered to possess various functions, including biosensing,[9] drug production,[14] chemical secretion,[15] and programed cell death.[16] On the other hand, the architectures of living materials and devices can be programed by 3D printing, including the microstructures of the hydrogel matrices, and the distribution of cells and chemicals within the matrices.[3,5] We can simulate the chemical diffusion and cell reaction in the 3D-printed living networks and predict the behaviors of living materials under various conditions.[17,18] In turn, the spatiotemporal responses of cells and matrices can provide rational feedback and guidance for the design of living materials and devices, thus enabling the programmable customization of living materials with predictable responsiveness.

X. Liu, H. Yuk, S. Lin, G. A. Parada, Prof. X. Zhao
Soft Active Materials Laboratory
Department of Mechanical Engineering
Massachusetts Institute of Technology
Cambridge, MA 02139, USA
E-mail: zhaox@mit.edu

G. A. Parada
Department of Chemical Engineering
Massachusetts Institute of Technology
Cambridge, MA 02139, USA

T.-C. Tang, E. Tham, Dr. C. de la Fuente-Nunez, Prof. T. K. Lu
Synthetic Biology Group
Research Laboratory of Electronics
Massachusetts Institute of Technology
Cambridge, MA 02139, USA

DOI: 10.1002/adma.201704821

T.-C. Tang, Dr. C. de la Fuente-Nunez, Prof. T. K. Lu
Department of Biological Engineering
Massachusetts Institute of Technology
Cambridge, MA 02139, USA

E. Tham
Department of Materials Science and Engineering
Massachusetts Institute of Technology
Cambridge, MA 02139, USA

Dr. C. de la Fuente-Nunez, Prof. T. K. Lu
Department of Electrical Engineering and Computer Science
Massachusetts Institute of Technology
Cambridge, MA 02139, USA

Prof. X. Zhao
Department of Civil and Environmental Engineering
Massachusetts Institute of Technology
Cambridge, MA 02139, USA

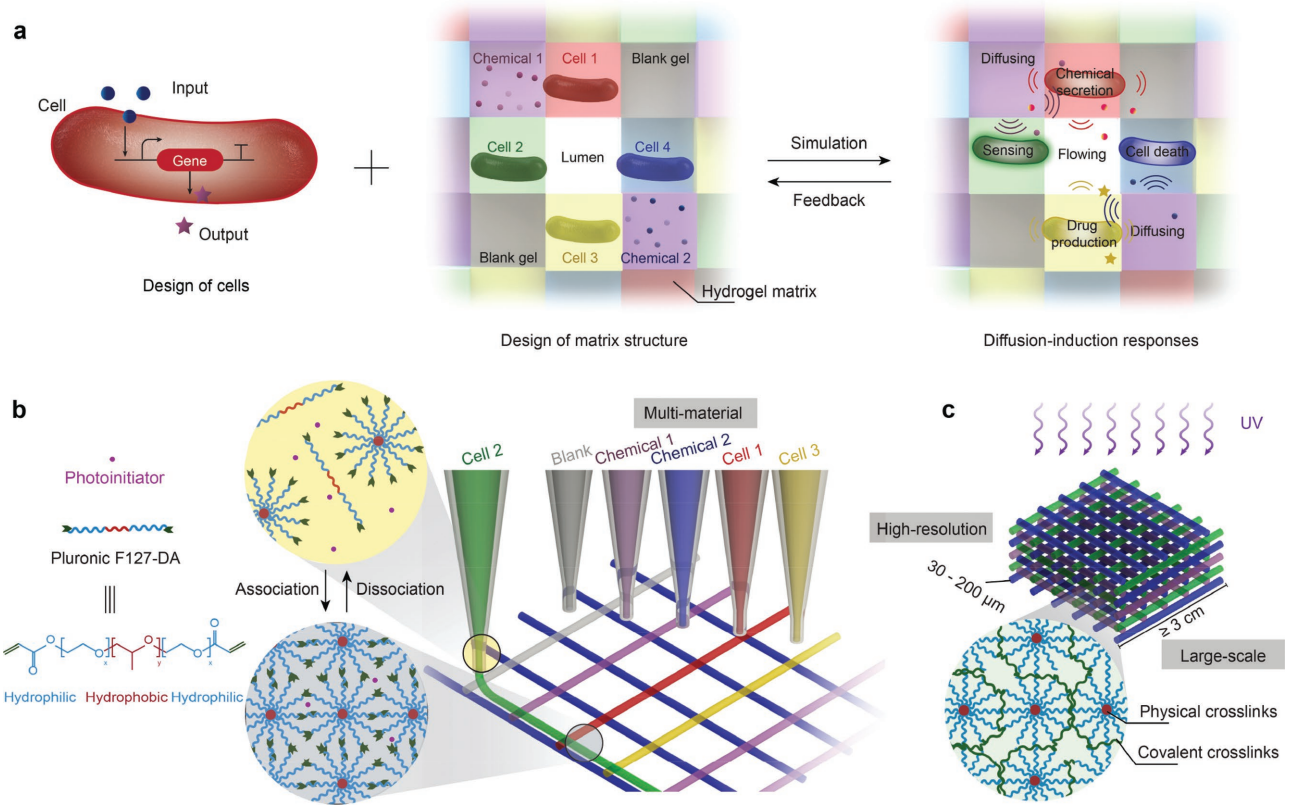

Figure 1. Design and 3D printing of large-scale, high-resolution living responsive materials and devices. a) Schematic workflow of living material design, which can be achieved by combined genetic circuit design in the encapsulated cells and structural design of living materials. The responses of living materials, including chemical diffusion and cell induction, can be predicted by simulation, which can provide feedback for living material design. b) Schematic illustration shows direct writing of hydrogel inks. The packing of Pluronic F127-DA micelles in the ink leads to a physically crosslinked hydrogel, which is fluidized by shear force during ink extrusion and recovers to the packing state right after printing. c) Schematic illustration shows that covalent crosslinks form among micelles after UV crosslinking. The fabrication processes b,c) result in a large-scale, high-resolution, and multiink living material.

Ink design is critical to ensure the viability and responsiveness of cells in living networks. Our ink system for 3D direct ink writing is based on a well-dispersed mixture of photoinitiator and polymeric micelles in water, with the addition of certain engineered bacterial cells, signaling chemicals, and nutrients. The components serve different purposes in the printing ink: Pluronic F127 diacrylate (Pluronic F127-DA) micelles provide ideal rheological behaviors required for direct ink writing, and the packing of Pluronic F127-DA micelles in the ink leads to a physically crosslinked hydrogel after printing[19]; Irgacure 2959 as photoinitiator allows postphotocrosslinking of the living structures after printing; engineered bacterial cells are programed to sense the signaling chemicals and respond with fluorescence and chemical secretion; signaling chemicals, including *N*-acyl homoserine lactone (AHL), isopropyl *β*-D-1-thiogalactopyranoside (IPTG), rhamnose (Rham), and anhydrotetracycline (aTc), are allowed to diffuse in the matrices and interact with different cell types; LB broth is used as the nutrient to maintain the viability and functionality of cells presented within matrices. Bacterial cells used in this study are engineered with different responsive functions: GFP+ strain expresses green fluorescence protein (GFP) constitutively; AHL/GFP+, Rham/GFP+, or IPTG/GFP+ strain produces GFP when chemical inducer AHL, Rham, or IPTG is received by the cognate cell strain, respectively; aTc/AHL+ strain secretes AHL when aTc is detected by the cell strain; AHL/GFP− strain can repress GFP production in cell when AHL is detected. In all, the living ink system provides a nourishing, biocompatible environment for cell survival and function (Figure 1b,c).

The 3D printing procedure for living materials consists of two steps: (i) direct writing of multiple hydrogel inks with various types of cells and chemicals (Figure 1b), and (ii) ultraviolet (UV) curing of the printed constructs (Figure 1c). During the direct ink writing, the nozzle diameter we adopt ranges from 30 to 200 μm, the nozzle feed rate is fixed at 5 mm s^{-1}, and the printing pressure is set as 90 kPa. We show that the mechanically reversible, rapidly responsive dissociation/association of Pluronic F127-DA micelles in water (Figure 1b) endows the ink with a strong shear-thinning effect during printing (Figure S2a, Supporting Information), and a plateau storage modulus (G′) orders of magnitude higher than loss modulus (G″) after printing (Figure S2b, Supporting Information). Thus, the Pluronic F127-DA micelles provide suitable rheological behaviors for 3D living printing. During UV irradiation, the printed sample is exposed to 1 J m^{-2} UV for 5 min.

The photocrosslinking is carried out under a humid nitrogen atmosphere to prevent hydrogel dehydration and oxygen inhibition of polymerization. The reactive end groups in Pluronic F127-DA enable the formation of covalent crosslinks among micelles after UV crosslinking (Figure 1c). The resultant hydrogel is mechanically robust and stretchable, with shear modulus of 50 kPa, toughness of 77 J m^{-2}, failure stretch of 162%, and fast recovery of elasticity within 1 min (Figure S3, Supporting Information). The mechanical robustness and structural integrity of hydrogel matrices can potentially enable applications of living devices that require mechanical reliability under cyclic deformation and robust integration with other engineering materials.[20–22]

To systematically evaluate the printability of the living ink, we vary the printing pressure and Pluronic F127-DA concentration in the ink, while fixing other parameters including nozzle diameter, nozzle feed rate, and ink compositions (e.g., cells, nutrients). We find the ink can be printed into 3D structures when the concentration of Pluronic F127-DA is between 18 and 36 wt% and the pressure is above a certain threshold, as shown in **Figure 2**a. When Pluronic F127-DA concentration is below 18 wt% or above 36 wt%, the ink cannot be printed due to liquid spreading or nozzle clogging, respectively; and when the printing pressure is below the threshold value, the ink cannot flow out of the nozzle (Figure 2a). In addition, we find that the printability of the ink is independent of nozzle dimensions (30–200 μm) for the ink composition used in this study (Figure 2a; Figure S4, Supporting Information).

To demonstrate the capability of printing large-scale and complex structures with multimaterial inks, various 3D architectures are printed (Figure 2b–f; Video S1, Supporting Information), including a cuboid, a pyramid, a dome, and hollow pyramids. The overall dimensions of the printed architectures can reach up to 3 cm. The first three cases (cuboid, pyramid, and dome, Figure 2b–d) show the capability of printing any solid constructs. In addition, the last two examples (hollow pyramids, Figure 2e,f) show that overhanging beams can be printed and the printed structures can be self-supporting due to the high yield stress of the ink materials (Figure S2b, Supporting Information). The multiple materials (red and green inks, Figure 2f) printed in selective regions of the last hollow pyramid demonstrate that our 3D printing technique is capable of integrating various types of cells and chemicals into a single construct. In addition, the 3D printing method can achieve very high spatial resolution as demonstrated in the printed grid microstructures with different local dimensions (Figure 2g–j). With encapsulated GFP+ bacterial cells, the grid microstructures of hydrogel matrices are clearly visualized under confocal microscope, with feature sizes varying from 200 μm (Figure 2g), 100 μm (Figure 2h), 50 μm

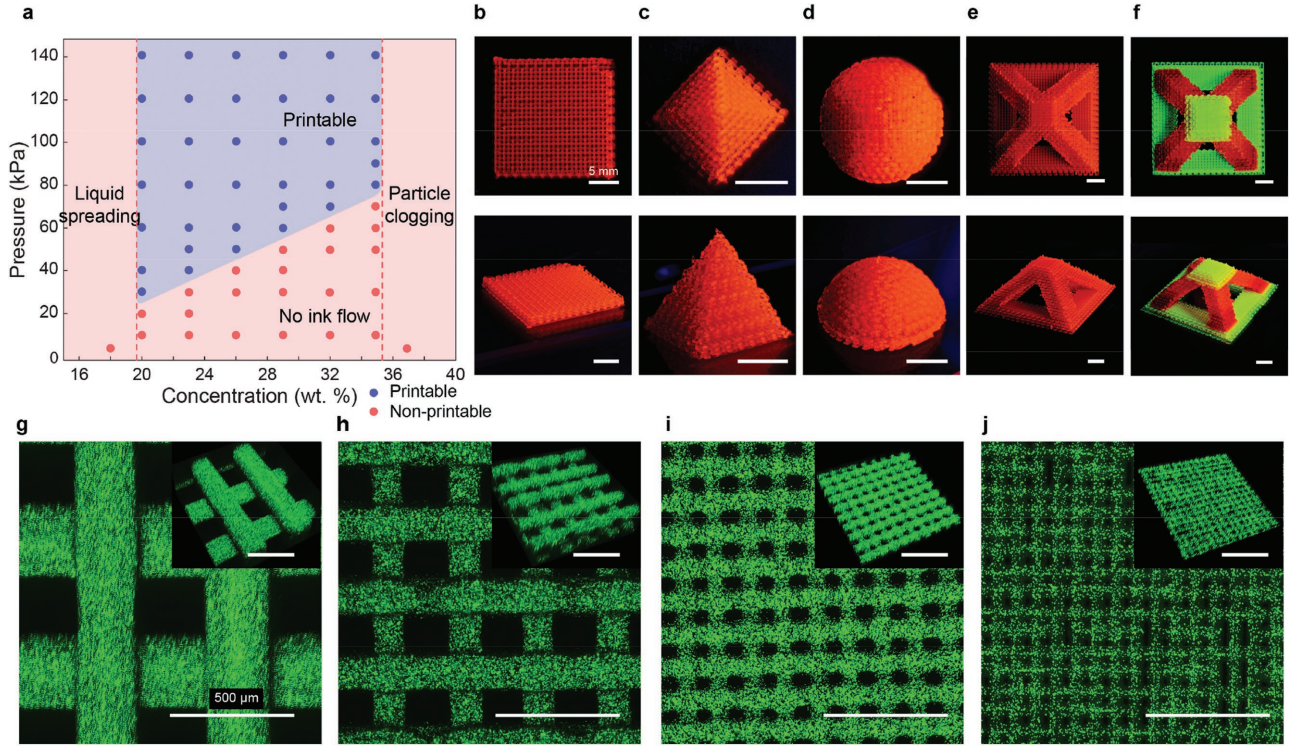

Figure 2. High printability of the hydrogel ink into large-scale, high-resolution structures with chemicals and bacterial cells. a) Phase diagram for the printability of Pluronic F127-DA ink. The ink can be printed into structures when the concentration of Pluronic F127-DA is between 18 and 36 wt% and the pressure is above a certain threshold as shown in (a). When Pluronic F127-DA concentration is below 18 wt% or above 36 wt%, the ink cannot be printed due to liquid spreading or particle clogging, respectively; and when the printing pressure is below the threshold value, the ink cannot flow out of the nozzle. Optical images of various architectures generated by 3D printing, including b) a cuboid, c) a pyramid, d) a dome, and e,f) hollow pyramids. Red color denotes hydrogel ink with rhodamine B, and green color denotes hydrogel ink with fluorescein (scale bars in (b)–(f), 5 mm). g–j) Confocal top-view images and 3D reconstructed images (insets) of GFP+ bacterial cell-laden hydrogel scaffolds with a wide range of printing resolutions, including g) 200 μm, h) 100 μm, i) 50 μm, and j) 30 μm (scale bars in (g)–(j), 500 μm).

(Figure 2i) to 30 µm (Figure 2j). Therefore, we can create complex macroscopic structures (3 cm) with microscopic precision (30 µm) through the 3D multimaterial printing method.

The 3D printing method and the ink materials can also give very high viability of bacterial cells in the printed living networks, due to the following reasons. First, all ink components including Pluronic F127-DA and Irgacure 2959 are biocompatible.[19,23] Second, the fabrication processes, including microextrusion (i.e., 90 kPa pressure) and UV irradiation (i.e., 1 J m^{-2} UV for 5 min) are mild for the encapsulated bacterial cells.[3] Bacterial cells with protective cell walls are able to survive relatively harsh conditions (such as shear force during extrusion and UV exposure during crosslinking) compared with more susceptible mammalian cells.[24] Third, hydrogel matrices can supply water and nutrients to cells, and ensure diffusion of signaling chemicals in the encapsulated multicellular system,[10] while fine features (30–200 µm) of the matrices allows for sufficient gas permeation.[25] To test cell viability in the hydrogel matrices, we use live/dead stain and fluorescence imaging for the cells in hydrogel matrices (200 and 100 µm in feature sizes). As shown in Figure S5 (Supporting Information), bacterial cells are highly viable (i.e., viability >95%) 24 h after printing. Therefore, the 3D printed microstructures provide a biocompatible, mechanically soft, and robust matrix that supplies nutrients and water for genetically engineered microorganisms, and ensures the successful operation of living materials over time.

The 3D printing of living materials and devices enables us to explore novel functions, including logic gates, spatiotemporally responsive patterning, and wearable devices. With the rapid development in synthetic biology, single cells have now been engineered to have new functions such as logic, memory, oscillator, and classifier.[9,13,26] To enable multicellular logic and guide signaling transmission for cell–cell communication, we print multiple types of cells and chemicals into 3D architectures and allow communication between different cell types to follow the well-defined networks of hydrogel matrices, thus achieving logic gates in the 3D-printed living materials and devices (**Figure 3**a,b). Each cell in the structure performs a simple computational operation. However, combined with their spatial distributions in the 3D architectures, the interactions among different cell types and chemicals in different regions can induce the emergence of informative patterns and achieve complex logic operations. For example, to perform single-input

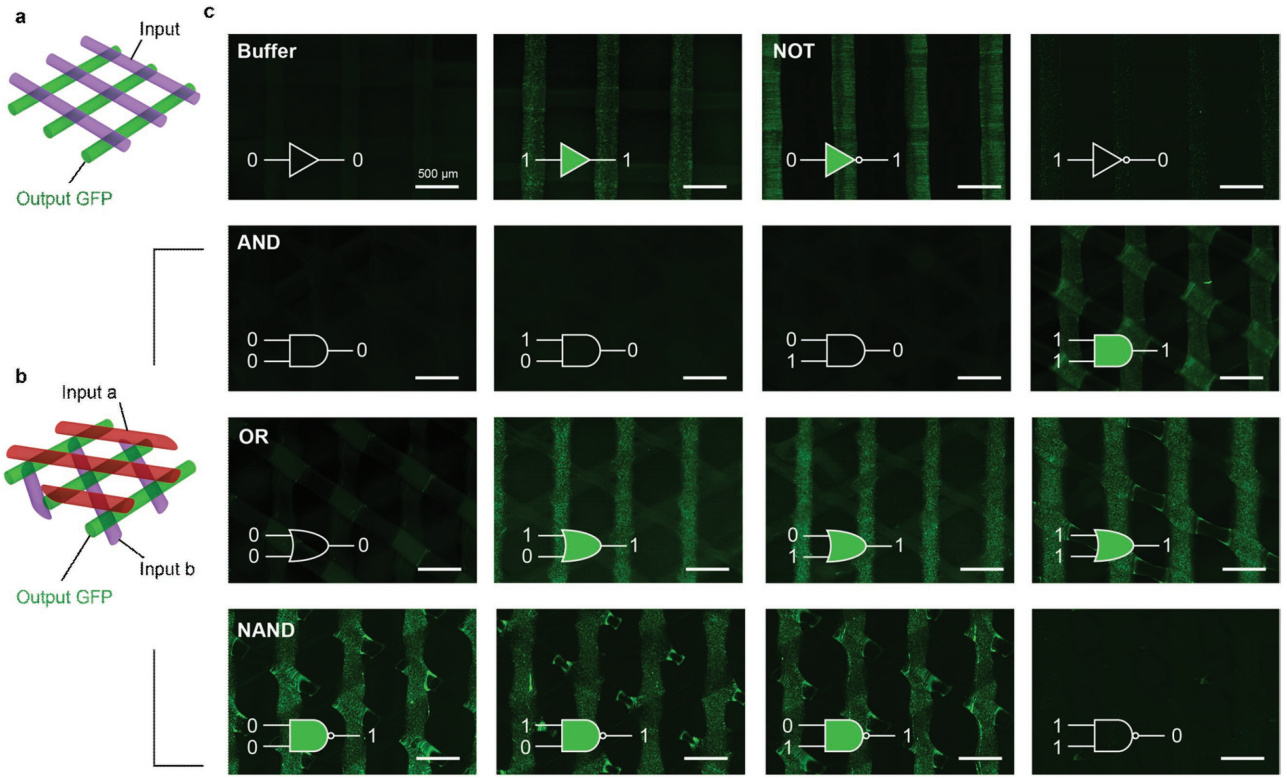

Figure 3. Logic gates achieved by multiink 3D printing of living materials. a) Schematic illustration of a 3D-printed living scaffold that can function as a single-input and single-output (SISO) Boolean logic gate. b) Schematic illustration of a 3D-printed living scaffold that can function as a double-input and single-output (DISO) Boolean logic gate. c) Experimental results of logic gates, indicated by green fluorescence in one layer of the printed hydrogel containing the output. The absence or presence of active components is denoted as 0 or 1 for inputs, while the absence or presence of GFP production is denoted as 0 or 1 for outputs. The input hydrogel layer remains dark no matter if it is 0 or 1, while the output hydrogel layer can be either green (1) or dark (0). The symbols (insets) show the inputs, computation, and outputs for each condition (scale bars in (c), 500 µm). Buffer gate input: AHL in hydrogel, output: AHL/GFP+ bacterial cells in hydrogel. NOT gate input: AHL in hydrogel, output: AHL/GFP– bacterial cells in hydrogel. AND gate inputs: aTc in hydrogel, aTc/AHL+ bacterial cells in hydrogel, output: AHL/GFP+ bacterial cells in hydrogel. OR gate inputs: AHL in hydrogel, Rham in hydrogel, output: a mixture of AHL/GFP+ bacterial cells and Rham/GFP+ bacterial cells in hydrogel. NAND inputs: aTc in hydrogel, aTc/AHL+ bacterial cells in hydrogel, output: AHL/GFP– bacterial cells in hydrogel.

and single-output (SISO) logic computation, we print orthogonally distributed hydrogel filaments; the rows contain chemicals which act as input, while the columns contain cells which act as output (Figure 3a,c). For double-input and single-output (DISO) Boolean logic gate, we print three types of crossed hydrogel filaments; the top ones contain input a, the bottom ones contain input b, and the columns in between contain cells which act as output (Figure 3b,c). The absence or presence of active components is denoted as 0 or 1 for inputs, while the absence or presence of GFP production is denoted as 0 or 1 for outputs. The input hydrogels remain dark no matter if they are 0 or 1, while the output hydrogel columns can be either green (1) or dark (0). As shown in Figure 3c and Table S1 in the Supporting Information, Buffer, NOT, AND, OR, and NAND gates are implemented by depositing different cells and chemicals in the constructs. In the Buffer gate, the output (AHL/GFP+ cells) is originally dark in the absence of AHL, while the presence of AHL can activate fluorescence in cells. In the NOT gate, the output (AHL/GFP− cells) is originally green in absence of NOT input, while the presence of an inhibitor (AHL) can repress GFP synthesis. In the AND gate, the AHL/GFP+ cells become green only when both input a (aTc) and input b (aTc/AHL+ cells) are present. In the OR gate, the output contains two cell types, AHL/GFP+ cells and Rham/GFP+ cells, and it turns on when either AHL or Rham is present. In the NAND gate, aTc and aTc/AHL+ cells act as two inputs which can induce the disappearance of green fluorescence in the output (AHL/GFP− cells). While logic gates that use nonliving chemicals or hydrogels have been reported,[27,28] here we demonstrate the first set of 3D-printed living logic gates using programed cells in hydrogels. These intricate structures, enabled by 3D multimaterial printing, provide well-organized, higher-level living cell networks that integrate multiple input signals for intelligent applications, including decision making and actuation in complex environments.[26]

Next, we demonstrate the capability of 3D-printed living materials to achieve spatiotemporally controlled patterning, owing to well-defined spatial distribution and time evolution in the living devices (Videos S2 and S3, Supporting Information). We choose two exemplary living patterns: a 1D pattern composed of cell parallel lines and a chemical perpendicular line (**Figure 4**a), and a 2D pattern composed of cell concentric rings with chemical radial lines (Figure 4e). The encapsulated cells we use in this particular experiment is AHL/GFP+ and the encapsulated chemical is AHL. For the 1D-living pattern, the set of experimental images (Figure 4b) reveal the spatiotemporal evolution of fluorescence in the living materials over 8 h. Similarly, the spatiotemporal fluorescence in the circular 2D-living pattern over 4 h is shown in the experimental images (Figure 4f). In both cases, the frontline of responded cells (i.e., turning fluorescent) within the hydrogel propagates along the paths of signaling chemical diffusion, and the fluorescence intensity of responded regions increases over time. We further develop a coupled diffusion–induction model that accounts for the chemical and cellular behaviors to predict the spatiotemporal responses of the living patterns. The prediction of the spatiotemporal patterns of the 3D-printed living materials relies on the understanding of two processes: (i) diffusion of signaling chemicals in hydrogel matrices and (ii) induction of encapsulated bacterial cells by signaling chemicals. The governing equations for these two processes are adopted from classical models[10,17] and given in the Supporting Information. To solve the governing equations, numerical models are developed for the living patterns using COMSOL Multiphysics with typical parameters listed in Table S2 in the Supporting Information. As shown in Figure 4b–d,f–h, the good agreement between experiments and simulations validates the predictability of our models. Therefore, the design of 3D living materials and devices can be rationally guided by such predictive models that account for the responses of cells and hydrogel matrices.

Besides the relatively planar structures with height of 400–600 μm shown in Figures 3 and 4, we further present a multilayer living responsive structure with height of 3.6 mm as illustrated in Figure S6a (Supporting Information). We print hydrogel inks that contain AHL and AHL/GFP+ cell in different regions of the 3D structure. Over time, the AHL molecules will diffuse from the AHL hydrogel region into the hydrogel region that contains AHL/GFP+ cells. Once the cells are induced (≈4 h after printing), the hydrogel region with cells in the living structure will become fluorescent (Figure S6b–c, Supporting Information).

The 3D printing of programed cells enables us to explore novel functions of living devices otherwise unachievable with structural design, printing fabrication, or genetic engineering alone. A living tattoo is designed to integrate a collection of multiple chemical-sensing cells (responsive to AHL, Rham, or IPTG) printed on the surface of a bilayer elastomeric sheet, and carefully attached to human skin (**Figure 5**a). The thin (≈75 μm), flexible, transparent, and gas permeable bilayer elastomeric sheet is fabricated by successive spin-coating deposition of two silicone elastomeric layers (Figure S7, Supporting Information), where the upper layer (Sylgard 184) is mechanically robust and flexible, and the lower layer (Silgel 613) is skin-adhesive which gives robust bonding to skin via van der Waals forces alone without the need for any additional fixtures or tapes (Figure 5a). The living device does not impose any mass loading on the skin nor mechanical constraint of the body motion.[29] As shown in Figure 5b, the skin can deform in different modes (i.e., stretching, compression, and twisting) freely and reversibly without any detachment of the living tattoo. Moreover, robust bonding between the hydrogel and the elastomer sheets and their mechanically soft nature prevents detachment (Figure S7, Supporting Information).[20,30] Further, the elastomer layer effectively reduces water loss from the printed hydrogel, and thus maintains cell viability and device functionality.[20] To examine practical applications of the living tattoo, three signaling chemicals (e.g., AHL, Rham, or IPTG) are smeared on the skin, respectively. When the chemicals are received, the adhered tattoos exhibit green fluorescence in corresponding 3D printed patterns. The monitoring of different chemicals by the living tattoo device on the skin is shown by experimental results (Figure 5c).

In summary, we report a new paradigm in 3D printing by using genetically programed cells as active components to create living materials and devices. This can be a new 4D-printing approach to produce 3D structures with time-evolving properties.[1–8] We elaborate design principles and general methods to print large-scale high-resolution living materials that are capable of integrating engineered cells

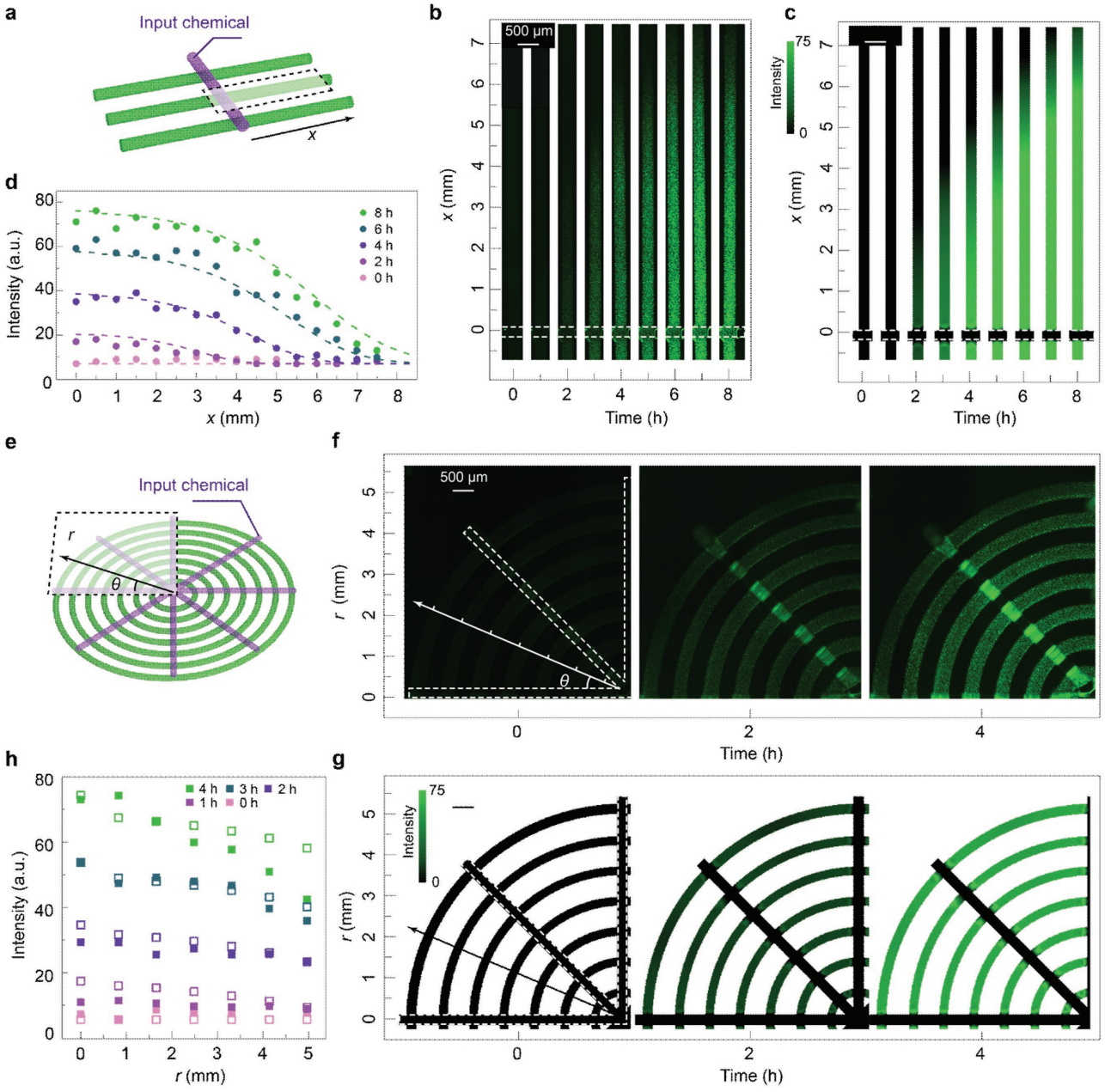

Figure 4. Spatiotemporal patterning of 3D-printed living materials. a) Schematic illustration of 1D-living structure. b) Spatiotemporal evolution of fluorescence in a straight line of the living structure (a) from experiments. c) Spatiotemporal evolution of fluorescence in a straight line of the living structure (a) from simulation. d) Quantitative comparison of fluorescence intensity over time in a straight line of the living structure (a) from experiments (solid dots) and simulations (dash lines). e) Schematic illustration of a 2D-living structure. f) Spatiotemporal evolution of fluorescence in a segment of the living structure (e) from experiments. g) Spatiotemporal evolution of fluorescence in a segment of the living structure (e) from simulation. h) Quantitative comparison of fluorescence intensity profiles over time along r in different rings of the living structure ($\theta = 22.5°$ in (e)) from experiments (solid squares) and simulations (hollow squares) (scale bars in (b), (c), (f), and (g), 500 μm).

into hydrogel constructs while maintaining high cell viability and ability to receive and process signals in a programmable manner. Novel applications enabled by 3D living printing of programed living cells are demonstrated, including logic gates, spatiotemporally responsive patterning, and wearable devices. The integrative technology of 3D living printing has the potential to be used as a general platform where a range of genetically programed cells (for example, cells with therapeutic production), matrices (for example, biodegradable hydrogels), and structures (for example, a cartilage shape) can be applied to design more customized living materials and devices with predictable dynamic functionalities. For instance, it is intriguing to envision a robust and personalized implant in which different cell types are programed to monitor inflammatory biomarkers and release growth factors to promote angiogenesis.[31,32] New ingestible devices based on our 3D printing of living materials

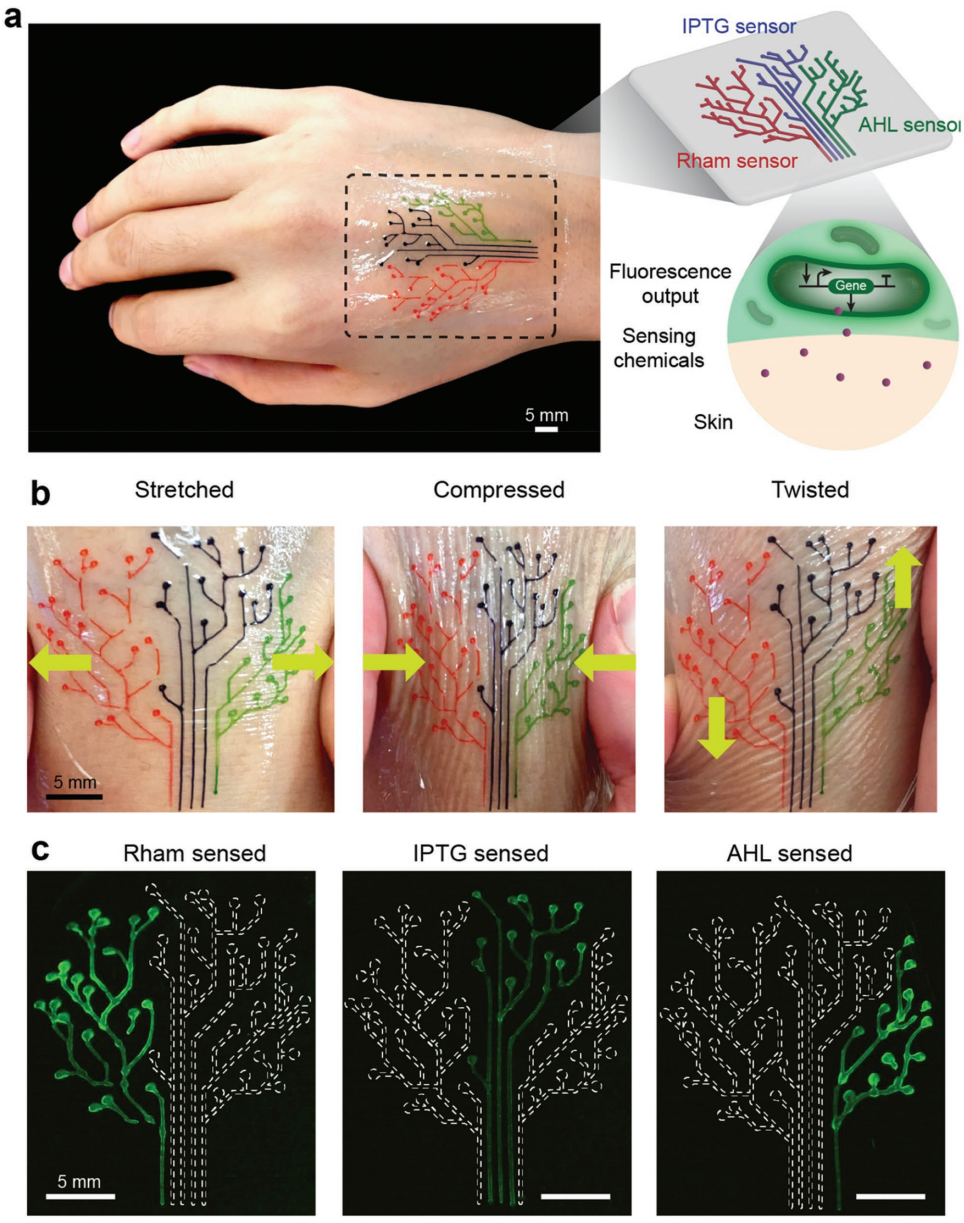

Figure 5. 3D-printed living tattoo for chemical detection on human skin. a) The design of the living tattoo. The tattoo is printed as a tree-like pattern on a thin elastomer layer, which is then adhered to human skin. Hydrogels with different colors illustrate the different types of cells encapsulated. Inset: Schematic illustration of living sensors embedded in the tattoo, which can respond to different chemicals by emitting fluorescence. b) The living tattoo on skin in different states: stretched (left), compressed (middle), and twisted (right). Food dyes are added to facilitate visualization of the hydrogel pattern in (a) and (b). c) The response of the living tattoo on the skin smeared with Rham (left), IPTG (middle), or AHL (right).

may be able to modulate the gut microbiota and treat microbe-mediated disease such as obesity and diabetes.[12] Overall, our 3D printing of living materials and devices opens new avenues toward real-world applications, such as on-demand medicine, biotechnology, bioremediation, and bioenergy via cell programing, structural design and direct ink writing technologies.

Experimental Section

The general procedures for creating 3D-printed living materials and devices involved the preparation of ink containing Pluronic F127-DA, photoinitiator, LB broth, antibiotic, chemical inducer, bacterial cell pellets, and deionized (DI) water. 3D architectures were printed at room temperature in air, and ultraviolet crosslinked after print completion. Samples were kept in a humid chamber. Unless otherwise specified, the chemicals used in the current work were purchased from Sigma-Aldrich and used without further purification.

Ink Preparation: The ink formulation for all experiments contained Pluronic F127-DA as polymer matrices, Irgacure 2959 as photoinitiator, LB broth (Miller) as nutrient, DI water, together with certain chemical inducers, antibiotics (i.e., carbenicillin), and/or bacterial cell pellets. Pluronic F127-DA was synthesized according to a reported protocol.[33] Briefly, 25 g of Pluronic F127 were dissolved into 80 mL of toluene at 60 °C under nitrogen with a condenser with circulating cold water. After 4 h, the solution was cooled down to room temperature, and then to 0 °C in an ice bath. 1.2 mL of trimethylamine was added to

the solution, followed by the dropwise addition of 0.5 mL of acryloyl chloride. The mixture was stirred overnight. Afterward, the precipitated byproduct was filtered away, and the solution was concentrated by rotary evaporator. The white product was precipitated from the viscous solution by adding hexane. Through a second filtration step and drying in a fume hood for 48 h, the Pluronic F127-DA product was obtained. The synthesized Pluronic F127-DA at 27 wt% concentration and Irgacure 2959 at 0.2 wt% were dissolved in DI water in the dark at 4 °C. Then, 0.25 wt% LB broth powder and 50 μg mL^{-1} carbenicillin were added to the mixture. Different active components, including chemical inducers (e.g., 100×10^{-9} M AHL, 1×10^{-3} M IPTG, 200 ng mL^{-1} aTc, and 12×10^{-3} M Rham) and cell pellets (e.g., AHL/GFP± cell, Rham/GFP+ cell, aTc/AHL+ cell, and GFP+ cell), were introduced in different ink systems. The cell density in the printing ink was ≈10^9 cells per mL. The freshly prepared inks were loaded into a UV-blocking 5 mL syringe barrel (EFD Nordson), and allowed to defoam at 4 °C for 1 h.

Printing and Crosslinking: The 3D living materials and devices were fabricated using a three-axis robotic deposition stage (Aerotech) by printing a 3D structure onto a glass slide (Corning) or a chambered coverglass (Lab-Tek) covered with a hydrophobic coating (Rain-X). The structures were designed using commercially available software including Solidworks (Dassault Systèmes) or CADfusion (Aerotech), and translated into G-code using a custom Python script. The prepared inks were housed in the 5 mL syringe barrels, which fitted with nozzles ranging in size from 30 μm (World Precision Instruments), 50 μm (Fisnar), 100 μm (Fisnar) to 200 μm (EFD Nordson). To achieve stable and optimal printing, we choose 90 kPa of air pressure (Ultimus V, Nordson EFD) as printing pressure, and 27 wt% Pluronic F127-DA in the ink for all experiments, where the printed hydrogel filaments are continuous and uniform, and their diameters are nearly the same as the nozzle diameters. After deposition, the physically crosslinked micelles was then chemically crosslinked by UV irradiation in a UV chamber (365 nm in wavelength, 1 J m^{-2}; UVP CL-1000) for 5 min, and the chamber was saturated with water vapor and nitrogen. After curing, the 3D structures were kept in a humid chamber.

Rheological Characterization: Ink rheology was measured using a controlled stress rheometer (AR-G2, TA Instruments) with a 40 mm diameter 2° cone-plate (54 μm gap) and parallel-plate geometry (250 μm gap). The rheology of chemically crosslinked hydrogel was measured using the same instrument with a 40 mm diameter parallel-plate geometry (3.2 mm gap). Shear viscosity measurements of ink were carried out in steady-state flow mode. The storage shear moduli of ink were measured using an oscillatory stress sweep at a frequency of 1 Hz. To study the time-dependent mechanical properties of physically crosslinked ink and chemically crosslinked hydrogel, the rheometer was used to measure the storage and loss shear moduli at different frequencies of oscillating strain ($\gamma = 0.01$). Measurements were carried out at 25 and 4 °C using an aqueous solvent trap to mitigate drying effects.

Mechanical Testing: The mechanical properties of chemically crosslinked hydrogel were further characterized by pure-shear test. The samples with dimensions of 50 mm in width, 10 mm in gauge length, and 1.5 mm in thickness were stretched at room temperature, using a mechanical testing machine (Z2.5, Zwick-Roell) with a 20 N load cell. One sample was notched with a crack and the others were unnotched. The notched sample was stretched to failure, and the unnotched samples were either stretched to failure or cyclically stretched to evaluate fracture toughness and energy dissipation.

Imaging and Image Analysis: Photographs of macroscopic 3D architectures were acquired using a DSLR camera (Nikon D7000). Fluorescent dyes, including Rhodamine-B and fluorescein (Sigma), and food dyes (McCormick) were used to improve visualization of hydrogel-printed structures. The microscopic hydrogel structures were imaged using an epifluorescence microscope (Nikon Eclipse LV100ND) or a confocal microscope (Nikon A1R). ImageJ was used to generate composite microscopy images by combining fluorescent channels. The fluorescence intensities were quantitatively measured using NIS-Element (Nikon).

Bacterial Strains and Plasmids: Plasmid construction and DNA manipulations were performed following standard molecular biology techniques (Figure S1, Supporting Information). We created plasmids containing different promoters, including the constitutive pGlpT, AHL-inducible pLux, Rham-inducible pRha, IPTG-inducible pLac, and aTc-inducible pTet. The transcript factors are constitutively expressed. Output genes, including *LuxI*, *cI*, *gfp,* and its derivatives, were tightly regulated by the inducible or constitutive promoters. Especially for AHL/GFP–, the cI/pLam invertor was cloned under the pLux promoter, and followed by a short-lived *gfp-LVA* reporter. The constructed plasmids were transformed into *E. coli* strain DH5αPRO using standard protocols.

Cell Viability Assay: 24 h after fabrication, the cell-laden hydrogels were peeled off from glass slides, and washed with 0.85% NaCl solution. Using the LIVE/DEAD BacLight bacterial viability kit, we stained the cells with SYTO 9 (5.01×10^{-6} M; Invitrogen) for live cells and propidium iodide (30×10^{-6} M; Invitrogen) for dead cells. 15 min after staining, fluorescent imaging of samples ($n = 3$) was carried out using an epifluorescence microscope (Nikon Eclipse LV100ND). Live and dead cell counts were obtained using the 3D objects counter plugin in ImageJ software.

Numerical Modeling: We developed a 2D finite-element model to simulate the chemical diffusion and cell induction in hydrogel patterns using COMSOL Multiphysics. Time-dependent transport of diluted species (tds) module as selected for the study. Parameters are shown in Table S2 (Supporting Information), and the geometries were the same as those in the experiments.

Living Tattoo Fabrication: The bilayer elastomeric sheet was fabricated by successive spin-coating deposition of two silicone elastomers, Sylgard 184 (Dow Corning) and Silgel 613 (Wacker). Sylgard 184 was first spin-coated on the glass at 1500 rpm for 60 s, and then cured at 70 °C for 1 h. Then, Silgel 613 was spin-coated on top of the Sylgard 184 at 1500 rpm for 60 s, and then cured at 70 °C for another 1 h. The elastomer surfaces were thoroughly cleaned with methanol and DI water, and completely dried with nitrogen gas before the benzophenone treatment. Thereafter, a benzophenone solution (10 wt% in ethanol) was applied onto the elastomer to evenly cover the entire elastomer surface for 1 min at room temperature. Then, the elastomer was washed with methanol three times and completely dried with nitrogen gas. The multiple hydrogel inks, which contain different cell sensors, were printed directly on the elastomer with 200 μm size nozzles, followed by 5 min UV curing, which led to the chemically crosslinked hydrogel and the robust bonding between hydrogel and elastomer. Lastly, we carefully peeled off the living tattoo from the glass slide, and adhered it on human skin for further testing.

All procedures involving human subjects conformed to the guidelines for protecting the rights of human subjects and were approved by the Massachusetts Institute of Technology Committee on the Use of Humans as Experimental Subjects (COUHES protocol No. 1701827491). All subjects provided informed consent.

Code Availability: G-code (print path) for all structures printed in Figures 2–5 is available on request.

Supporting Information

Supporting Information is available from the Wiley Online Library or from the author.

Acknowledgements

X.L. and H.Y. contributed equally to this work. The authors thank Dr. Eliza Vasile and Dr. Hon Fai Chan for help with confocal imaging. This work is supported by ONR (Grant No. N00014-14-1-0528), NSF (Grant No. CMMI-1253495, MCB-1350625, Expeditions in Computing Program 1522074), NIH (Grant No. 1P50GM098792, DTRA (Grant No. HDTRA1-15-1-0050) and MIT Institute for Soldier Nanotechnologies. X.Z. acknowledges the financial support from Draper Laboratory. H.Y. acknowledges the financial support from Samsung Scholarship. C.F.N. acknowledges the funding from Ramon Areces Foundation (Spain).

Conflict of Interest

The authors declare no conflict of interest.

Keywords

3D printing, living materials, spatiotemporal patterning, wearable living sensors

Received: August 23, 2017
Revised: September 22, 2017
Published online:

[1] B. Gao, Q. Yang, X. Zhao, G. Jin, Y. Ma, F. Xu, *Trends Biotechnol.* **2016**, *34*, 746.
[2] C. Norotte, F. S. Marga, L. E. Niklason, G. Forgacs, *Biomaterials* **2009**, *30*, 5910.
[3] D. B. Kolesky, K. A. Homan, M. A. Skylar-Scott, J. A. Lewis, *Proc. Natl. Acad. Sci. USA* **2016**, *113*, 3179.
[4] A. Sydney Gladman, E. A. Matsumoto, R. G. Nuzzo, L. Mahadevan, J. A. Lewis, *Nat. Mater.* **2016**, *15*, 413.
[5] G. Villar, A. D. Graham, H. Bayley, *Science* **2013**, *340*, 48.
[6] T. A. Campbell, S. Tibbits, B. Garrett, *Sci. Am.* **2014**, *311*, 60.
[7] Z. Pei, Y. Yang, Q. Chen, E. M. Terentjev, Y. Wei, Y. Ji, *Nat. Mater.* **2014**, *13*, 36.
[8] Z. Ding, C. Yuan, X. Peng, T. Wang, H. J. Qi, M. L. Dunn, *Sci. Adv.* **2017**, *3*, e1602890.
[9] A. S. Khalil, J. J. Collins, *Nat. Rev. Genet.* **2010**, *11*, 367.
[10] X. Liu, T.-C. Tang, E. Tham, H. Yuk, S. Lin, T. K. Lu, X. Zhao, *Proc. Natl. Acad. Sci. USA* **2017**, *114*, 2200.
[11] G. I. Evan, K. H. Vousden, *Nature* **2001**, *411*, 342.
[12] R. E. Ley, P. J. Turnbaugh, S. Klein, J. I. Gordon, *Nature* **2006**, *444*, 1022.
[13] P. Siuti, J. Yazbek, T. K. Lu, *Nat. Biotechnol.* **2013**, *31*, 448.
[14] P. Perez-Pinera, N. Han, S. Cleto, J. Cao, O. Purcell, K. A. Shah, K. Lee, R. Ram, T. K. Lu, *Nat. Commun.* **2016**, *7*, 12211.
[15] Y. Chen, J. K. Kim, A. J. Hirning, K. Josić, M. R. Bennett, *Science* **2015**, *349*, 986.
[16] M. O. Din, T. Danino, A. Prindle, M. Skalak, J. Selimkhanov, K. Allen, E. Julio, E. Atolia, L. S. Tsimring, S. N. Bhatia, *Nature* **2016**, *536*, 81.
[17] G. E. Dilanji, J. B. Langebrake, P. De Leenheer, S. J. Hagen, *J. Am. Chem. Soc.* **2012**, *134*, 5618.
[18] E. Karzbrun, A. M. Tayar, V. Noireaux, R. H. Bar-Ziv, *Science* **2014**, *345*, 829.
[19] D. B. Kolesky, R. L. Truby, A. Gladman, T. A. Busbee, K. A. Homan, J. A. Lewis, *Adv. Mater.* **2014**, *26*, 3124.
[20] H. Yuk, T. Zhang, G. A. Parada, X. Liu, X. Zhao, *Nat. Commun.* **2016**, *7*, 12028.
[21] H. Yuk, T. Zhang, S. Lin, G. A. Parada, X. Zhao, *Nat. Mater.* **2016**, *15*, 190.
[22] X. Zhao, *Proc. Natl. Acad. Sci. USA* **2017**, *114*, 8138.
[23] I. Mironi-Harpaz, D. Y. Wang, S. Venkatraman, D. Seliktar, *Acta Biomater.* **2012**, *8*, 1838.
[24] S. Hong, D. Sycks, H. F. Chan, S. Lin, G. P. Lopez, F. Guilak, K. W. Leong, X. Zhao, *Adv. Mater.* **2015**, *27*, 4035.
[25] R. L. Truby, J. A. Lewis, *Nature* **2016**, *540*, 371.
[26] Z. Xie, L. Wroblewska, L. Prochazka, R. Weiss, Y. Benenson, *Science* **2011**, *333*, 1307.
[27] H. Komatsu, S. Matsumoto, S.-i. Tamaru, K. Kaneko, M. Ikeda, I. Hamachi, *J. Am. Chem. Soc.* **2009**, *131*, 5580.
[28] M. Ikeda, T. Tanida, T. Yoshii, K. Kurotani, S. Onogi, K. Urayama, I. Hamachi, *Nat. Chem.* **2014**, *6*, 511.
[29] D.-H. Kim, N. Lu, R. Ma, Y.-S. Kim, R.-H. Kim, S. Wang, J. Wu, S. M. Won, H. Tao, A. Islam, *Science* **2011**, *333*, 838.
[30] G. A. Parada, H. Yuk, X. Liu, A. J. Hsieh, X. Zhao, *Adv. Healthcare Mater.* **2017**, *6*, 1700520.
[31] J. L. Drury, D. J. Mooney, *Biomaterials* **2003**, *24*, 4337.
[32] X. Zhao, J. Kim, C. A. Cezar, N. Huebsch, K. Lee, K. Bouhadir, D. J. Mooney, *Proc. Natl. Acad. Sci. USA* **2011**, *108*, 67.
[33] F. Cellesi, N. Tirelli, J. A. Hubbell, *Macromol. Chem. Phys.* **2002**, *203*, 1466.

ADVANCED MATERIALS

Supporting Information

for *Adv. Mater.*, DOI: 10.1002/adma.201704821

3D Printing of Living Responsive Materials and Devices

*Xinyue Liu, Hyunwoo Yuk, Shaoting Lin, German Alberto Parada, Tzu-Chieh Tang, Eléonore Tham, Cesar de la Fuente-Nunez, Timothy K. Lu, and Xuanhe Zhao**

Supporting Information

3D Printing of Living Responsive Materials and Devices

*Xinyue Liu, Hyunwoo Yuk, Shaoting Lin, German Alberto Parada, Tzu-Chieh Tang, Eléonore Tham, Cesar de la Fuente-Nunez, Timothy K. Lu, Xuanhe Zhao**

X. Liu, H. Yuk, S. Lin, G. A. Parada, Prof. X. Zhao
Soft Active Materials Laboratory, Department of Mechanical Engineering, Massachusetts Institute of Technology, Cambridge, MA 02139, USA
E-mail: zhaox@mit.edu
G. A. Parada
Department of Chemical Engineering, Massachusetts Institute of Technology, Cambridge, MA 02139, USA
T. Tang, E. Tham, C. Fuente-Nunez, Prof. T. K. Lu
Synthetic Biology Group, Research Laboratory of Electronics, Massachusetts Institute of Technology, Cambridge, MA 02139, USA
T. Tang, C. Fuente-Nunez, Prof. T. K. Lu
Department of Biological Engineering, Massachusetts Institute of Technology, Cambridge, MA 02139, USA
E. Tham
Department of Materials Science and Engineering, Massachusetts Institute of Technology, Cambridge, MA 02139, USA
Dr. C. Fuente-Nunez, Prof. T. K. Lu
Department of Electrical Engineering and Computer Science, Massachusetts Institute of Technology, Cambridge, MA 02139, USA
Prof. X. Zhao
Department of Civil and Environmental Engineering, Massachusetts Institute of Technology, Cambridge, MA 02139, USA

Development of the model for living materials

Quantifying the operation of 4D printed living materials requires a general model that accounts for the transportations of chemicals and the responses of cells in the materials[1-3]. The chemical diffusion in the hydrogel matrices is taken to follow the Fick's law[2]

$$\frac{\partial C}{\partial t} = -D\nabla C \tag{1}$$

where C is the moles of the signaling chemicals per unit volume of hydrogel (i.e., chemical concentration), t is the current time, and D is the diffusion coefficient of the chemical in hydrogel. The biochemical reactions in cells depend on the genetic circuits of different cell types. For the inducible GFP expression in cells, we adopt the induction model in previous works, which considers the processes of immature protein synthesis, protein maturation, cell division, and protein degradation[2, 4]. We denote the numbers of immature protein and mature protein in a cell as n and f, respectively, and the numbers of cell per unit volume (i.e., cell density) in the hydrogel as N. Their rates of variation can be expressed as[2, 3]

$$\frac{\partial n}{\partial t} = P_m \cdot \frac{C^h}{C^h + K^h} - m \cdot n - \mu \cdot (1 - \frac{N}{N_m}) \cdot n - k \cdot n \tag{2}$$

$$\frac{\partial f}{\partial t} = m \cdot n - \mu \cdot (1 - \frac{N}{N_m}) \cdot f - k \cdot f \tag{3}$$

$$\frac{\partial N}{\partial t} = \mu \cdot (1 - \frac{N}{N_m}) \cdot N \tag{4}$$

where P_m is the maximum rate of immature GFP expression, h is the Hill coefficient, K is the half-maximal parameter, m is the maturation constant, μ is the cell growth constant, N_m is the maximum cell density in hydrogel, and k is the degradation constant. Note that the measurable

fluorescence intensity in the hydrogel is the number of fluorescent protein per unit of volume in hydrogel, that is $N \cdot f$.

Table S1. Input and output chemicals or cells for logic gate construction.

Gate	Input a	Input b	Output
Buffer	AHL (100 nM)	/	AHL/GFP+ cells
NOT	AHL (100 nM)	/	AHL/GFP cells
AND	aTc (200 ng/mL)	aTc/AHL+ cells	AHL/GFP+ cells
OR	AHL (100 nM)	Rham (12 mM)	AHL/GFP+ cells Rham/GFP+ cells
NAND	aTc (200 ng/mL)	aTc/AHL+ cell	AHL/GFP cells

Table S2. Parameter values for the spatiotemporal model in Fig. 4. These values are adopted from our previous paper[2].

Parameter	Definition	Value
D	diffusion coefficient of the chemical in hydrogel	2.0×10^{-10} m^2/s
C_0	initial chemical concentration in hydrogel with chemical	200 nM
P_m	maximum rate of immature GFP expression	1000 s^{-1}
h	Hill coefficient	1.66
K	half-maximal parameter	1.5 nM
m	maturation constant	1.16×10^{-3} s^{-1}
μ	cell growth constant	1.20×10^{-4} s^{-1}
N_m	maximum cell density in hydrogel	3.5×10^{8} cells/ml
k	degradation constant	2.0×10^{-5} s^{-1}
n_0	initial immature protein in a cell	0
f_0	initial mature protein in a cell	0
N_0	initial cell density in hydrogel	1.6×10^{8} cells/ml

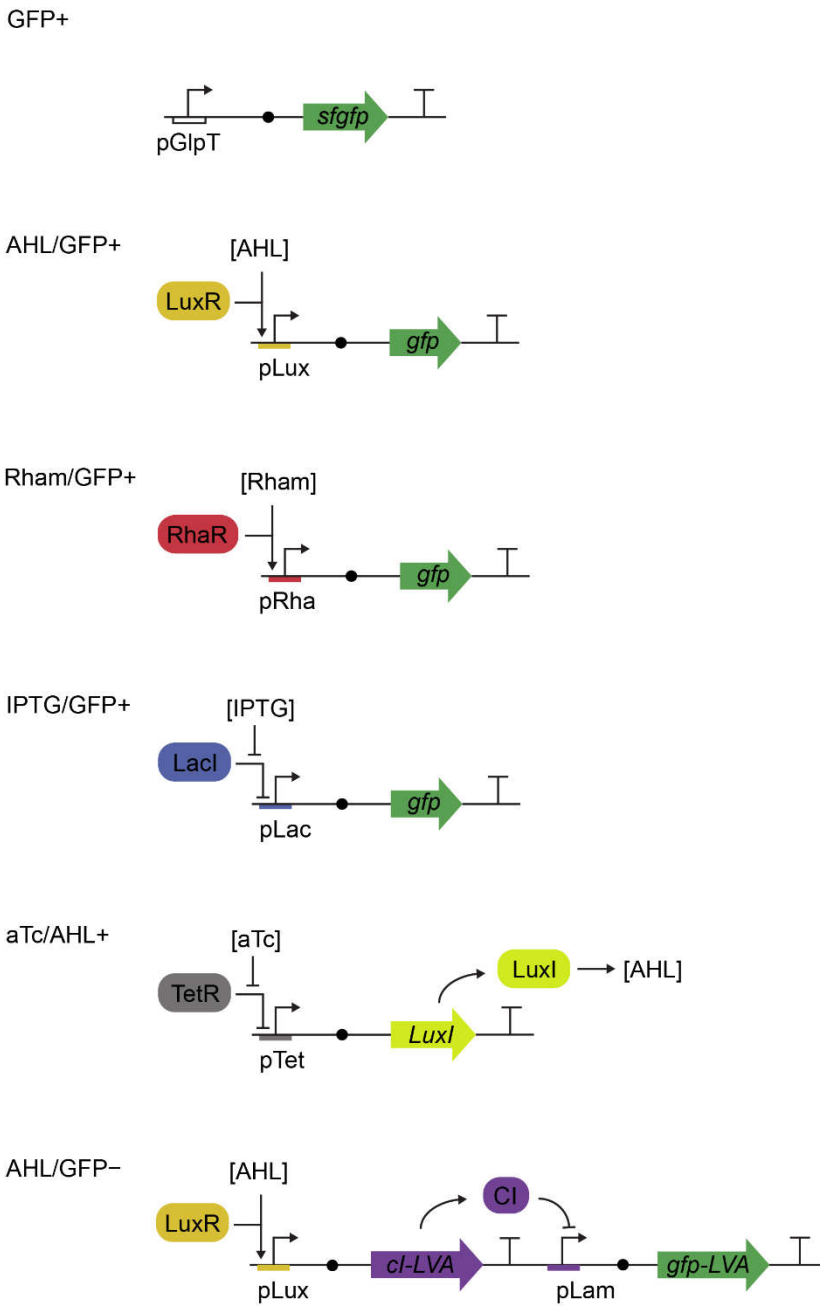

Figure S1. Circuit diagrams of the engineered bacterial strains. The inducers (such as AHL, Rham, IPTG, and aTc) interact with transcriptional factors (such as, LuxR, RhaR, LacI, and TetR, respectively), and induce downstream gene expression. pGlpT is a constitutive promoter. cI/pLam repressor module acts as a invertor for GFP expression in the cell. *sfgfp* denotes a gene for

superfolder GFP. *LVA* denotes a gene for protein degradation tag, which reduce the GFP half-life from two days to two hours.

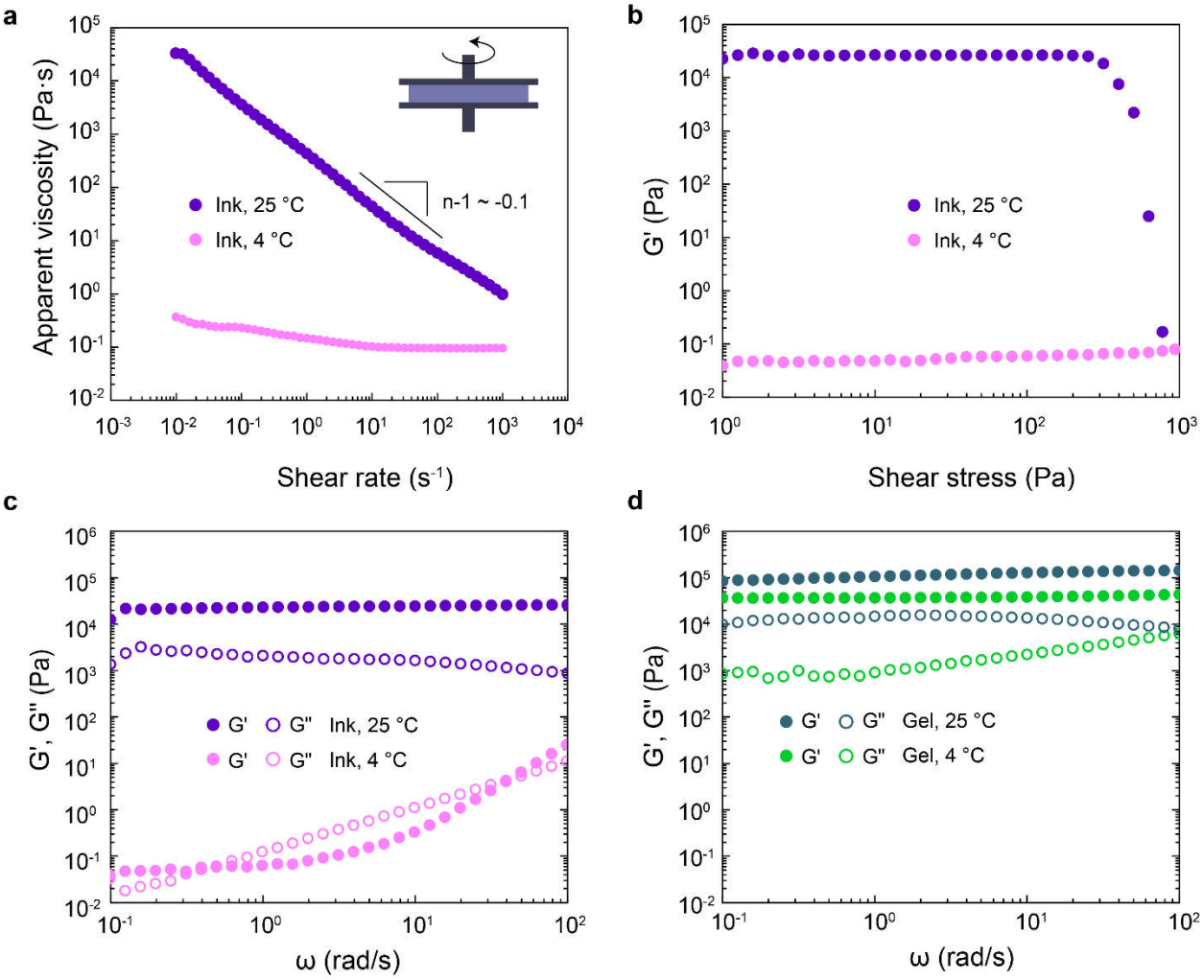

Figure S2. Rheological behavior of Pluronic F127-DA ink and UV-crosslinked hydrogel. a) Ink apparent viscosity as a function of shear rate at 25°C and 4°C. b) Ink shear storage moduli (G') as a function of shear stress at 25°C and 4°C, measured in oscillatory mode at 1 Hz. c) Ink shear storage moduli (G', solid dots) and loss moduli (G", open dots) as a function of angular velocity (ω) at 25°C and 4°C. d) UV crosslinked hydrogel shear storage moduli (G', solid dots) and loss moduli (G", open dots) as a function of angular velocity (ω) at 25°C and 4°C.

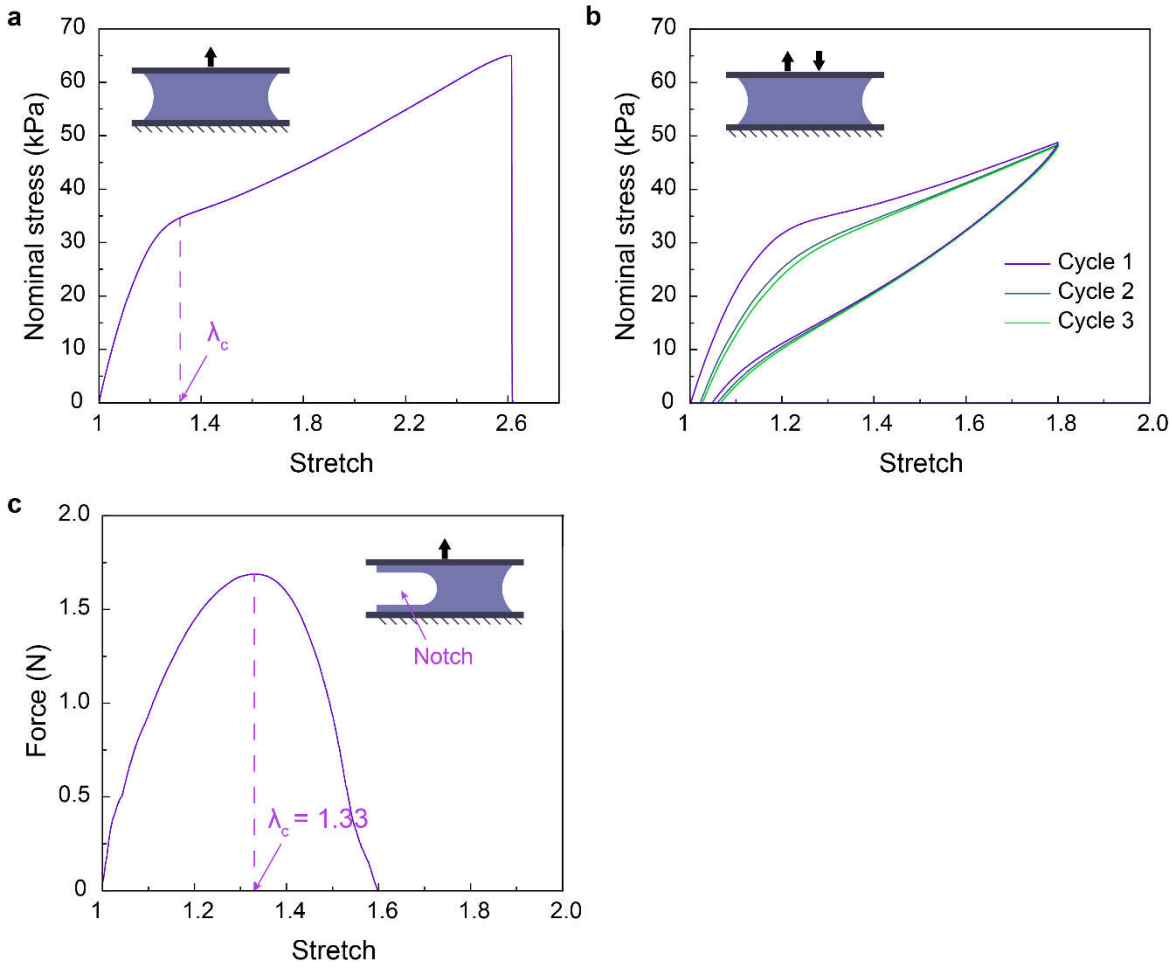

Figure S3. Mechanical behavior of Pluronic F127-DA UV-crosslinked hydrogel. a) Stress–stretch curve of the hydrogel. b) Cyclic stress-stretch curve measured by loading and unloading the hydrogel to a stretch of 1.8. Three cycles are carried out. c) Stress–stretch curve of the notched hydrogel. The critical stretch for steady crack propagation measured in notched samples is indicated as λ_c.

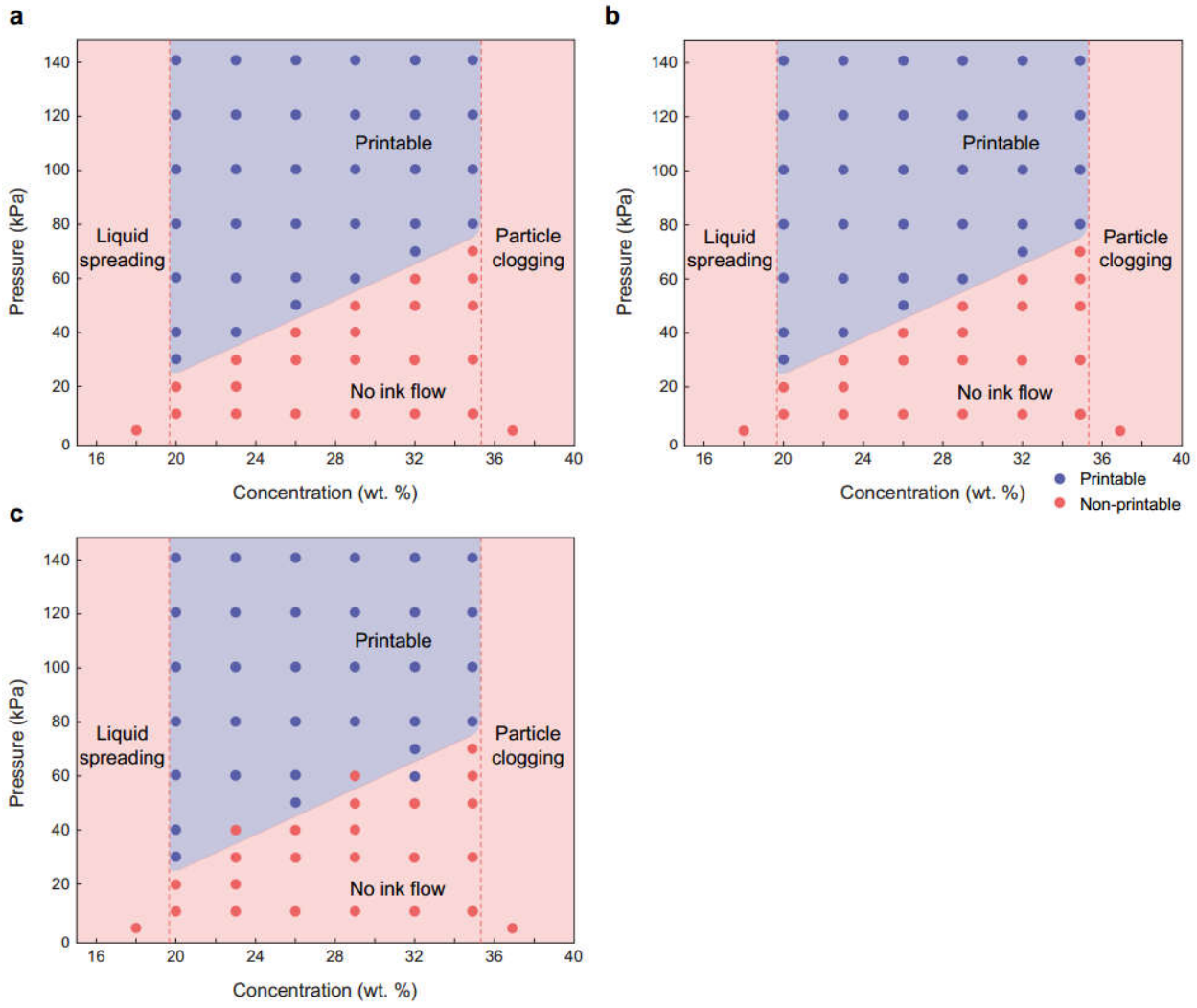

Figure S4. Printability diagrams with different nozzle dimensions. a-c) Phase diagrams for Pluronic F127-DA ink printability, which contains non-printable (red) and printable (blue) regions. The tests are carried out with 200 μm (a),100 μm (b), and 30 μm (c) in nozzle size.

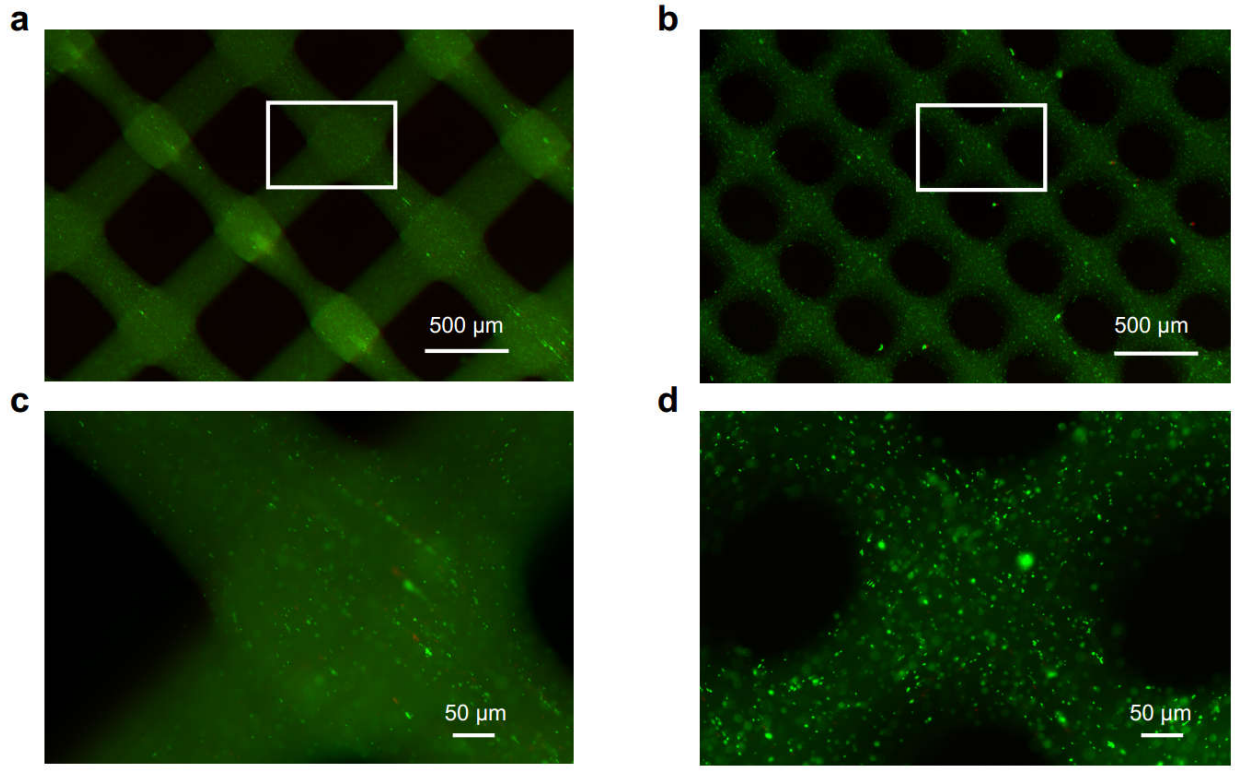

Figure S5. Cell viability in Pluronic F127-DA UV-crosslinked hydrogel tested by live-dead assay 24 h after printing. a,c) Fluorescent images of bacterial cells in printed living materials with 200 µm feature size. b,d) Fluorescent images of bacterial cells in printed living materials with 100 µm feature size. Red denotes dead cells (resulting from increased uptake of propidium iodide into membrane damaged/dead cells), while green denotes live cells. Scale bars are shown in images.

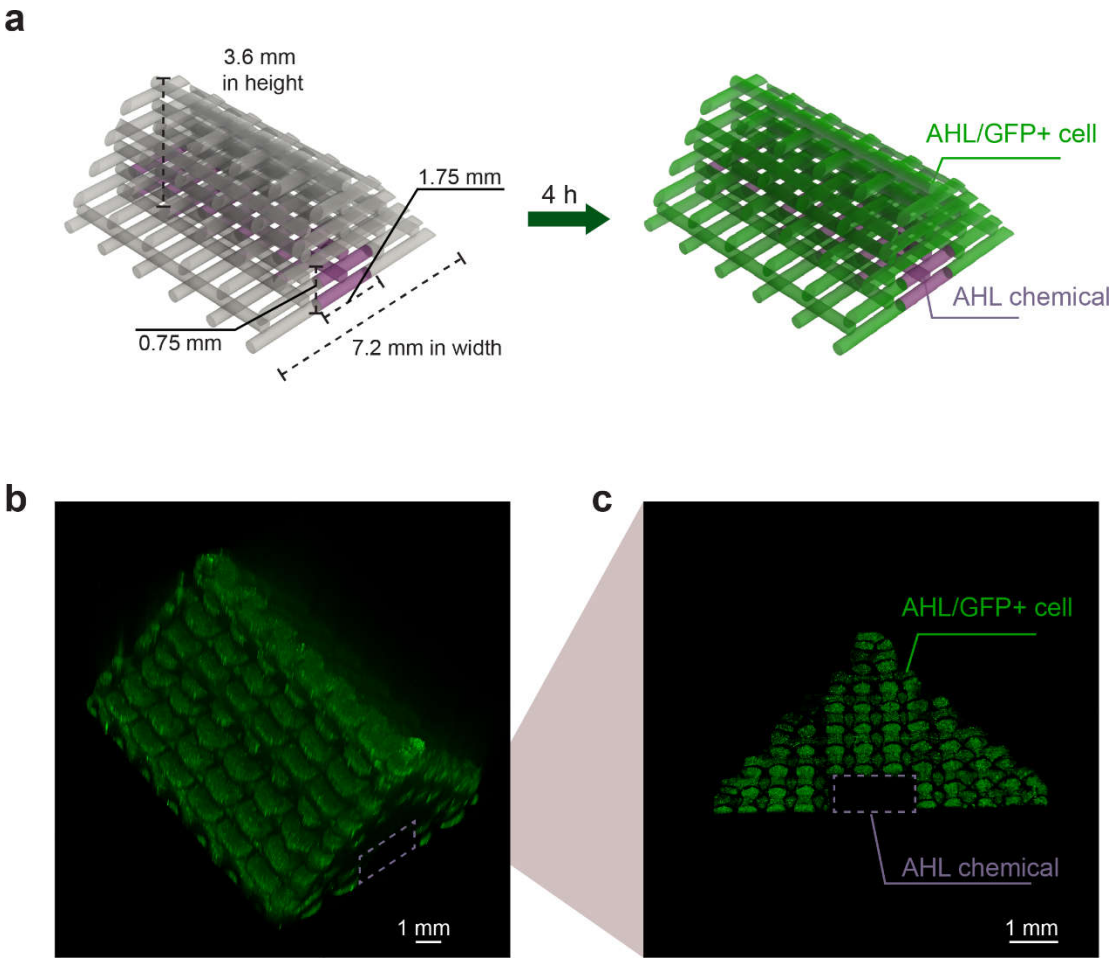

Figure S6. 3D patterning of a living structure. a) Schematic illustration of a 3D living structure (3.6 mm in height). The hydrogel inks contain AHL and AHL/GFP+ cell in different regions of the 3D structure. Once the cells are induced (~4 hours after printing), the hydrogel region with cells in the living structure become fluorescent. b) 3D reconstructed fluorescent images and c) cross-section fluorescent images of a the 3D living structure with 18 layers of hydrogel deposition. Scale bar in b-c, 1mm.

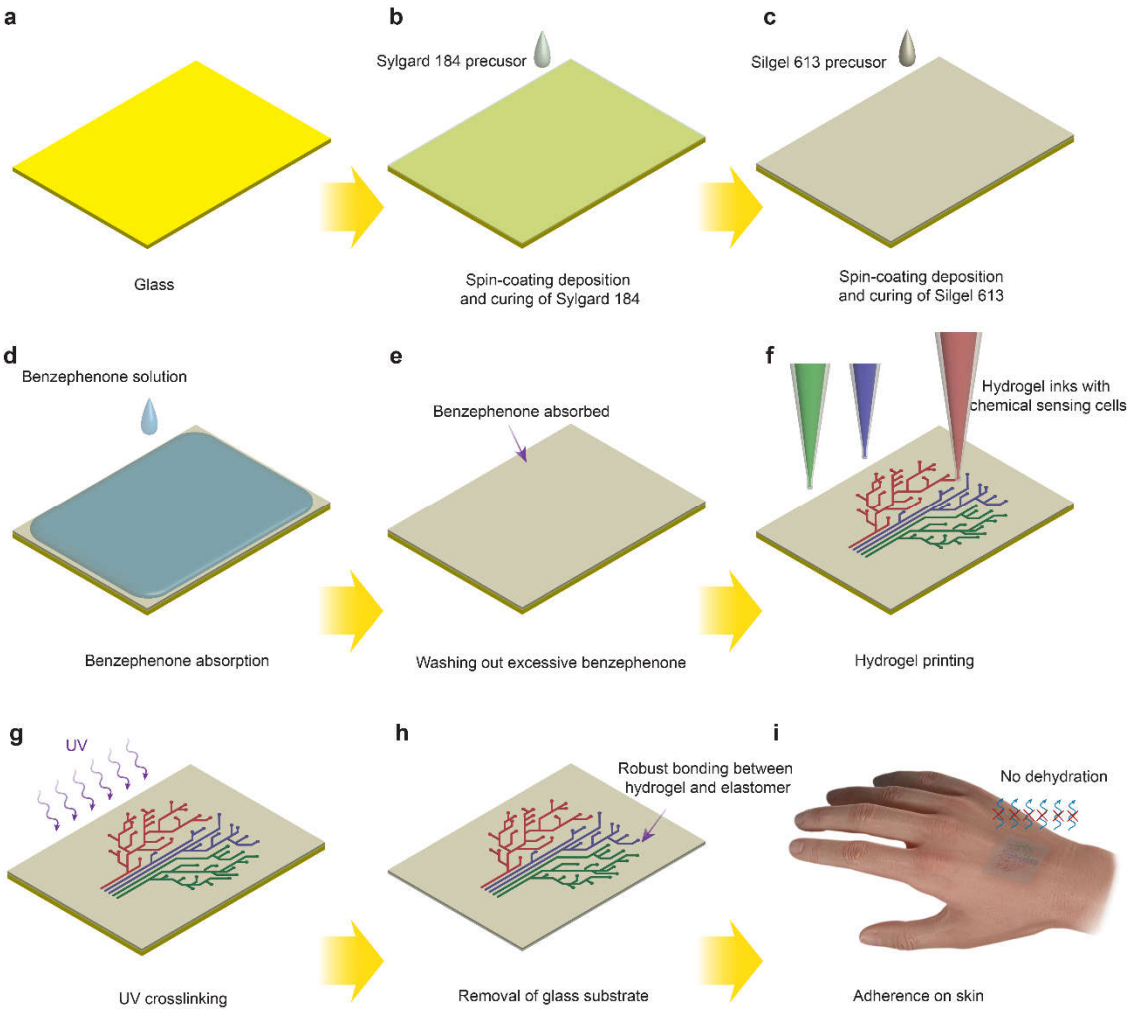

Figure S7. Schematic illustration of living tattoo fabrication. a-c) Spin-coating and curing of two types of elastomeric thin films on glass substrate. d,e) Surface activation of elastomer by benzophenone solution. f) Printing of hydrogel inks containing bacterial cells on the elastomer. g) Hydrogel crosslinking and surface bonding by UV irradiation. h,i) Removal of the glass substrate and adherence of the living tattoo to skin.

SUPPLEMENTARY MOVIE CAPTIONS

Video S1: The multimaterial direct ink writing process (speed × 16) of a living material with a 3D structure.

Video S2: The multimaterial direct ink writing process (speed × 4) of a living material with a 2D tree-like pattern.

Video S3: Spatiotemporal responses of a living material with the 2D tree-like pattern over three hours.

References

[1] A. M. Tayar, E. Karzbrun, V. Noireaux, R. H. Bar-Ziv, *Nature Physics* **2015**, 11, 1037.
[2] X. Liu, T.-C. Tang, E. Tham, H. Yuk, S. Lin, T. K. Lu, X. Zhao, *Proc. Natl. Acad. Sci. USA* **2017**, 114, 2200.
[3] G. E. Dilanji, J. B. Langebrake, P. De Leenheer, S. J. Hagen, *Journal of the American Chemical Society* **2012**, 134, 5618.
[4] J. H. Leveau, S. E. Lindow, *Journal of bacteriology* **2001**, 183, 6752.